A decoupling-design strategy for high sound absorption in subwavelength structures with air ventilation

Cite as: JASA Express Lett. **2**, 033602 (2022); https://doi.org/10.1121/10.0009919
Submitted: 20 December 2021 • Accepted: 09 March 2022 • Published Online: 25 March 2022

Ruojun Zhang, Guibo Wang, Xiaoming Zhou, et al.

JASA EXPRESS LETTERS ARTICLE asa.scitation.org/journal/jel

A decoupling-design strategy for high sound absorption in subwavelength structures with air ventilation

Ruojun Zhang,[1,a)] Guibo Wang,[2] Xiaoming Zhou,[1,b)] and Gengkai Hu[1]
[1]Key Laboratory of Dynamics and Control of Flight Vehicle, Ministry of Education and School of Aerospace Engineering, Beijing Institute of Technology, Beijing 100081, China
[2]Research Center on Shipbuilding Applied Acoustic, China Shipbuilding Information Center, Beijing 100101, China
ruojunzhang@126.com, csic_wangguibo@126.com, zhxming@bit.edu.cn, hugeng@bit.edu.cn

Abstract: A strategy based on the decoupling design of two elementary structures, both made of coiled-up channels, is proposed. One channeling structure is designed for blocking sound transmission, while the other element is used for absorbing sounds at low-transmission frequencies. Based on this strategy, the sound-absorbing sample with air ventilation is fabricated and its high-absorption capability is demonstrated experimentally. The expanding of sound absorption bandwidth by combining different absorptive channels into the sample structure is also demonstrated. The proposed method provides a new route towards broadband high sound absorption in ventilated structures.

[Editor: Tracianne B. Neilsen] https://doi.org/10.1121/10.0009919

Received: 20 December 2021 **Accepted:** 9 March 2022 **Published Online:** 25 March 2022

1. Introduction

Absorption of audible sounds by materials and/or structures of subwavelength scale is a long-standing interest in wide branches of wave physics due to both its scientific challenge and engineering demand. Among diverse models, the structure embedded with cavities and channels offers the great design flexibility to tailor sound propagation losses, and has been proven valid in achieving either sound insulation or absorption while maintaining the subwavelength geometry.[1–4] For the one-port system terminated by rigid backings, the sound absorption problem refers to the issue of how to remove the wave reflected from the backing side. This could be achieved by matching the input impedance of control materials to the air in as wide a frequency range as possible using Fabry–Pérot channels[5,6] and Helmholtz resonators.[7] By contrast, in the two-port system that allows the flow of air through it, the challenge of perfect acoustic absorption relies on the fact that the transmission and reflection of sounds must be eliminated simultaneously. For a thin layer whose thickness is far less than the operating wavelength, there exists a critical coupling condition, which results in the fact that the limit of maximum sound absorption is 0.5.[8] Great efforts have been devoted to reach high absorption beyond this limit in recent years.

Several models have been proposed for sound absorption in ventilated structures.[9–21] For instance, perfect sound absorption can be achieved through mirror-symmetric and anti-symmetric resonances by using a pair of degenerated monopole and dipole resonators of subwavelength dimensions,[9,22] or through the rainbow trapping of sounds in an array of Helmholtz resonators with graded dimensions.[20] Efficient sound absorption is also available through the hybridization of different eigenmodes in two layers of split tube resonators,[10,18] decorated thin membranes resonators,[21] Helmholtz resonators,[12–17] coiled-up Fabry–Pérot resonators,[11] and micro-perforated plates.[19] For either degenerate or hybrid resonance mechanisms, perfect sound absorption requires the delicate regulation of two or more absorptive elements. In this study, we propose a different strategy to achieve high sound absorption in two-port systems. In this strategy, one structure is designed for blocking the wave transmission yet with the air flow, while the other structure is designed for absorbing sounds. The reflective and absorptive structures can be designed separately using this strategy, which lifts the restriction on the delicate manipulation of functional structures. Results will be demonstrated by both theoretical and experimental analyses.

2. Methods

We begin with a straight waveguide internally coupled to a rigidly backed coiling channel of cross sectional area S_2 and length L_2, as illustrated in Fig. 1(a). Effective length of the coiling channel relative to the waveguide is denoted by L_1.

[a)]Also at: Research Center on Shipbuilding Applied Acoustic, China Shipbuilding Information Center, Beijing 100101, China.
[b)]Author to whom correspondence should be addressed.

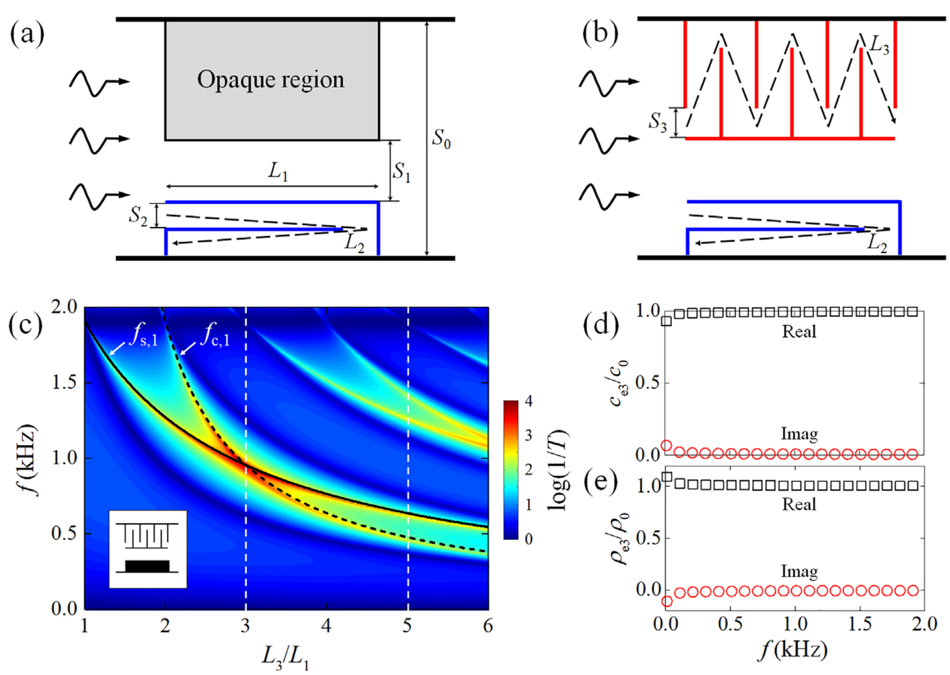

Fig. 1. Theoretical model. (a) A ventilated waveguide inserted with a rigidly backed coiling channel for achieving sound absorption, (b) combined with another channeling structure with open ends on both sides used for reflection of sounds, (c) contour plot of acoustic transmission T against the variation of the frequency f and length ratio L_3/L_1. The line plots refer to the curves $f_{s,m} = mc_0/(L_3 + L_1)$ and $f_{c,n} = (n - 1/2)c_0/(L_3 - L_1)$, where $m = n = 1$ is chosen, (d) normalized effective sound velocity c_{e3}/c_0, and (e) effective density ρ_{e3}/ρ_0 of reflective channels for different frequencies.

The cross sectional area of the upstream/downstream part of the waveguide is denoted by S_0, and the area of the ventilated part is S_1. Sound transmission coefficient is given by (see the supplementary material[23])

$$T_a = \frac{2Z_2/Z_0}{\left(2\frac{Z_2}{Z_0} + \frac{S_2}{S_0}\right)\cos k_0L_1 + i\left(\frac{S_0}{S_1}\frac{Z_2}{Z_0} + \frac{S_2}{S_1} + \frac{S_1}{S_0}\frac{Z_2}{Z_0}\right)\sin k_0L_1}, \tag{1}$$

where $k_0 = \omega/c_0$ and $Z_0 = \rho_0c_0$. Z_2 refers to the input impedance of the coiling channel, and is given by $Z_2 = -iZ_{e2}\cot(\omega L_2/c_{e2})$,[24] where Z_{e2} and c_{e2} are effective impedance and effective sound velocity, respectively (see the supplementary material[23]) and they have incorporated the effect of viscous damping of air inside narrow channels. Now, let us analyze the case that the ventilated part is of subwavelength size, i.e., $k_0L_1 \ll 1$, then it follows from Eq. (1) that $T_a = 2Z_2/(2Z_2+Z_0S_2/S_0)$. According to Eq. (1), the condition to diminish the transmission is to let $Z_2 = 0$. The imaginary part of Z_2 can be made zero at a particular resonant frequency. However, the real part of Z_2 (acoustic resistance) is the non-zero value, describing the acoustic damping caused by the visco-thermal effect in micro channels. This concludes the fact that high sound absorption is hard to achieve by subwavelength side branches with damping.

In this work, we made an effort to overcome this limitation by combining the absorptive channel with another channeling structure capable of strong sound reflection, as depicted in Fig. 1(b). The reflective structure is a space-coiling channel of cross sectional area S_3 and length L_3 with open ends on both sides. The general expression of acoustic transmission T and reflection coefficient R of the composite structure is given by (see the supplementary material[23])

$$T = \frac{2\alpha}{(1+\beta)\left[1+\beta+A_2Z_0/(\phi_2Z_{e2})\right] - \alpha^2}, \tag{2a}$$

$$R = \frac{(1+\gamma)\phi_2Z_{e2} - A_2Z_0}{(1-\gamma)\phi_2Z_{e2} + A_2Z_0} \tag{2b}$$

with

$$\alpha = A_1\xi_1 + A_3\xi_3\frac{Z_0}{Z_{e3}}, \quad \beta = A_1\phi_1 + A_3\phi_3\frac{Z_0}{Z_{e3}}, \quad \gamma = \frac{\alpha^2}{1+\beta} - \beta,$$
$$\xi_1 = \frac{1}{i\sin k_0L_1}, \quad \xi_3 = \frac{1}{i\sin k_3L_3}, \quad \phi_j = -i\cot k_jL_j \ (j = 1, 2, 3),$$

where $Z_0 = \varrho_0c_0$, $A_j = S_j/S_0$, $k_1 = k_0 = \omega/c_0$, $k_2 = \omega/c_{e2}$, and $k_3 = \omega/c_{e3}$. Z_{e3} and c_{e3} represent the effective characteristic impedance and effective sound velocity of thin-sized channeling structure (see the supplementary material[23]). From Eq. (2a), the transmission T can be diminished if the numerator is zero, namely $\alpha = 0$; this condition is only related to the modulation of reflective channels, irrespective to the absorption channels. At low-transmission frequencies corresponding to $\alpha = 0$, the reflection R can be further lowered by modulating the absorptive channels, according to Eq. (2b). So, it is possible to implement the decoupling design of reflective and absorptive channels to achieve high sound absorption of ventilated structures.

3. Results and discussions

Let us proceed with the analyses using numerical examples. Consider first the case whereby there is only the reflective channel with parameters $L_1 = 90$ mm, $S_0 = 80 \times 80\,\mathrm{mm}^2$, $S_3 = 10 \times 25\,\mathrm{mm}^2$, $S_1 = S_3$, and $S_2 = 0$. Figure 1(c) shows the contour plot of the transmission T against the variation of the frequency f and length ratio L_3/L_1. The trajectories of transmission dips can be clearly observed. Based on the fact that the imaginary parts of both effective sound velocity and density of reflective channels are very small as presented in Figs. 1(d) and 1(e), we assume that the reflective channel is free of damping, having $c_{e3} = c_0$ and $\rho_{e3} = \rho_0$, in order to illustrate how the trajectory correlates to the zero-transmission condition, $\alpha = 0$. In that case, we have $Z_{e3} = Z_0$, and the condition of $\alpha = 0$ leads to $\sin[k_0(L_3 + L_1)/2]\cos[k_0(L_3 - L_1)/2] = 0$. The explicit relations between the frequency f and length L_3 of reflective channels can then be identified and expressed by two sets of equations $f_{s,m} = mc_0/(L_3 + L_1)$ and $f_{c,n} = (n - 1/2)c_0/(L_3 - L_1)$, herein m and n are positive integer values. In fact, these two frequencies $f_{s,m}$ and $f_{c,n}$ are relevant to local monopolar and dipolar modes of the channel with open ends.[25] Consider the lowest order modes $m = n = 1$, the frequencies $f_{s,1}$ and $f_{c,1}$ against the length ratio L_3/L_1 have been plotted in Fig. 1(c), showing the excellent agreement with the transmission-dip trajectories. This confirms our prediction that the transmission drop is just relevant to the modulation of reflective channels.

Next, let us analyze acoustic responses of composite structures with both reflective and absorptive channels. We begin with a special case by setting the length ratio $L_3/L_1 = 3$. At this case, the zero-transmission condition $\alpha = 0$ results in the same frequencies $f_{s,1}$ and $f_{c,1}$, both equaling $c_0/(4L_1)$. The reflection coefficient R in Eq. (2b) is simplified as $R = (Z_2 - Z_0A_2)/(Z_2 + Z_0A_2)$. This equation is in exactly the same form to the reflection of the composite structure in which the opening of both reflective and ventilated channels is rigidly blocked. The reflection can then be readily diminished using the absorptive channel. Despite the fact that the damping of reflective channels is neglected in the above example and the result is restricted to the special case $L_3/L_1 = 3$, the decoupling-design strategy disclosed here can be extended to the more general scenarios with damping and arbitrary length ratio L_3/L_1 as addressed below. It is seen from Fig. 1(c) that the length ratio L_3/L_1 affects the transmission-dip frequencies in an inversely proportional manner. Without loss of generality, we consider the case $L_3/L_1 = 5$. Figure 2(a) shows the frequency spectrum of acoustic transmission, reflection, and absorption of the composite without absorptive channels. Compared to the case of $L_3/L_1 = 3$, the extremely low transmission below 0.01 can be observed in a finite frequency band from 420–705 Hz (solid line). Importantly, this low-transmission behavior also can be predicted by the non-damping model (dashed line), showing the weak dependence on the damping effect. One could also understand this behavior from Fig. 1(c), where the low-transmission region corresponds to the frequency range between $f_{c,1} < f < f_{s,1}$. It is noteworthy that the low transmission is caused by the strong reflection rather than the sound dissipation as shown in Fig. 2(a). At low-transmission frequencies, we employ absorptive channels to further reduce the sound reflection. According to Eq. (2b), the sound reflection R can be removed by equating its numerator to zero, obtaining the zero-reflection condition $(1 + \gamma)\phi_2 Z_{e2} = A_2 Z_0$, where γ are known parameters relevant

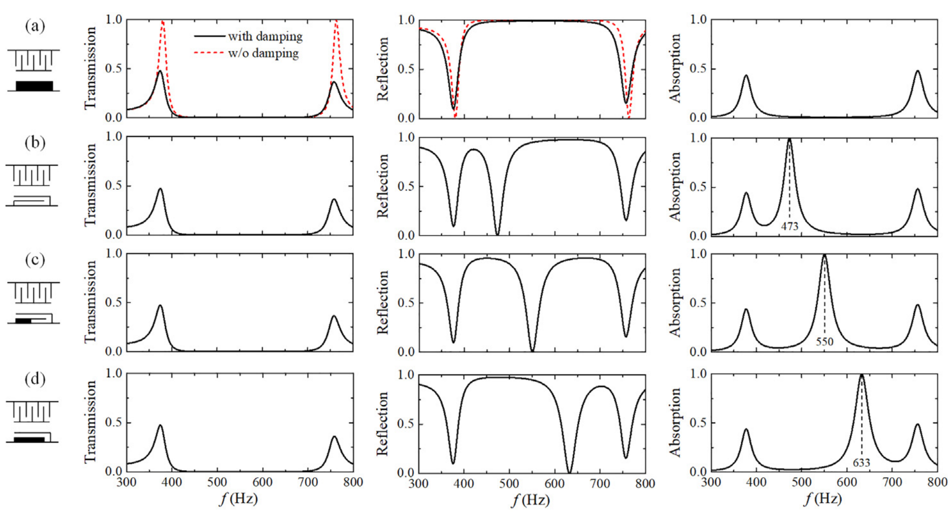

Fig. 2. Frequency spectrum of acoustic transmission, reflection, and absorption of the composite with only reflective channels (a), and added with absorptive channels [(b)–(d)] capable of high sound absorption at frequencies 473, 550, and 633 Hz, respectively.

to the reflective channel. Using this condition, the geometry of absorptive channels can then be determined for a given frequency. As examples, we choose three different frequencies 473, 550, and 633 Hz, all falling within the low-transmission region. The geometric parameters of absorptive channels are determined as $L_2 = 178.42$ mm, $S_2 = 28 \times 5.7\ \mathrm{mm}^2$; $L_2 = 153.57$ mm, $S_2 = 28 \times 5.4\ \mathrm{mm}^2$; $L_2 = 133.75$ mm, $S_2 = 28 \times 5.2\ \mathrm{mm}^2$, respectively. Acoustic responses of composite structures with three types of absorptive channels are shown in Figs. 2(b)–2(d). When absorptive channels are included, the spectrum profile of acoustic transmission remains nearly unchanged, while the reflection has been greatly reduced at the target frequency. Eventually, the high sound absorption is achieved as a result of reduction of both sound transmission and reflection. To sum up, the reflective channel is designed according to the zero-transmission condition $\alpha = 0$, and is used for the transmission reduction. The absorptive channel functions for further reducing the sound reflection at the transmission-dip frequencies, and it can be designed based on the zero-reflection condition $(1+\gamma)\phi_2 Z_{e2} = A_2 Z_0$. For the proposed model, the reflective and absorptive channels can be designed separately, allowing the decoupling-design strategy to be adopted for achieving the high sound absorption.

Based on the decoupling-design strategy, we have designed and fabricated the sound-absorbing sample as shown in Fig. 3(a). The sample consists of a hollow cavity for air ventilation, and deposited on one side of the cavity is the coiled rectangular cross sectional duct used for sound reflection. Three types of absorptive channels with different working frequencies 404.5, 432.5, and 455.5 Hz are placed compactly on the other side (see the supplementary material[23] for their geometric parameters). The sample is fabricated by the 3 D printing using ABS (acrylonitrile butadiene styrene plastic) materials, which can be considered to be rigid with respect to air. We first evaluate the sound transmission, reflection, and absorption of the sample without absorptive channels by blocking their entrances with rigid panels, as shown in Fig. 3(b). Experimental results show the near-zero transmission near frequencies 404.5 and 715 Hz, as well as the very low transmission between them. Notice that the low transmission in this broad frequency range is induced by the strong reflection instead of the intrinsic viscous damping as indicated in the figure. To realize the high sound absorption at low-transmission frequencies, we open separately each absorptive channel and measure acoustic responses of composite structures as shown in Figs. 3(c)–3(e). In the presence of absorptive channels, the sound transmission spectrum remains nearly

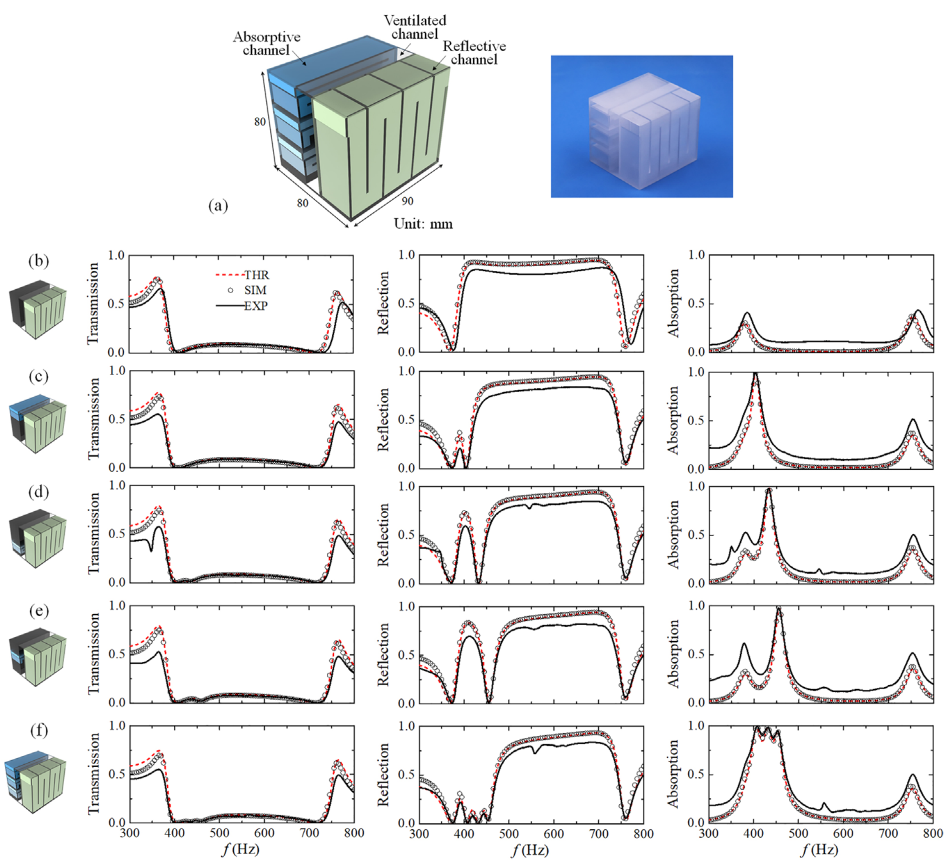

Fig. 3. (a) The schematic and photograph of the sound-absorbing sample that comprises one reflective channel and three absorptive channels with different working frequencies. (b)–(f) Theoretical, simulation, and experimental results of acoustic responses of the sample in five cases. (b) No absorptive channels operate. (c)–(e) Only one absorptive channel operates. (f) Three absorptive channels operate simultaneously.

unchanged while high sound absorption has been realized at the target frequency, clearly demonstrating the decoupling-design strategy.

Acoustic performances of the sample structure are also verified by finite-element simulations based on software package COMSOL Multiphysics. To simulate the viscous damping of the air within the channels, the viscous-thermal losses are taken into account using the Narrow Region Acoustics module. Simulation results have been presented in Fig. 3, where theoretical predictions based on Eq. (2) are provided as well. Theoretical, simulation, and experimental results of peak absorption frequency coincide very well and their spectrum profiles are in good agreement. With the aid of simulation results in Figs. 3(c)–3(e), we provide a deep analysis of underlying mechanisms of nearly total absorption at target frequencies 404.5, 432.5, and 455.5 Hz by plotting acoustic pressure fields at the respective vertical mid-plane of absorptive, ventilated, and reflective channeling structures, as shown in Figs. 4(a)–4(c). In all three cases, antisymmetric scattering behavior is clearly observed at inlet and outlet regions of reflective channels. The absorptive channel with a rigid end is known to affect the incident wave by the monopole scattering, and is characterized by symmetric behavior in the vicinity of its inlet. Thus, the maximum absorption attained here may be understood by the critical coupling between the symmetric and antisymmetric resonances. This is consistent with the observation in mirror-symmetric acoustic metascreens,[9] where perfect absorption has been achieved based on this mechanism. Although the studied system is not mirror symmetric, the critical coupling behavior can still be observed, demonstrating the generalization of this concept.

Figure 3(f) shows acoustic responses of the sample when three absorptive channels operate simultaneously. Measured sound absorption is greater than 0.8 in the frequency range 396–461 Hz, demonstrating the superposition effect of individual channels for the widening of the absorption bandwidth. Notice that the sample thickness is 90 mm, which is nearly $\frac{1}{8.4}$ wavelength of air corresponding to the band center frequency 428.5 Hz. So, the high sound absorption by ventilated structures of subwavelength size has been clearly demonstrated. One might be able to further broaden the absorption bandwidth by packing more absorptive channels.

The air ventilation performance of the sample structure is studied by numerical simulations based on the computational fluid dynamics (CFD) module in COMSOL Multiphysics (see the supplementary material for modeling details[23]). Figure 4(d) shows the averaged outlet flow velocity against the variation of inlet velocities for systems with and without the sample structure. It is seen that the flow velocity at the outlet region increases with an increase in input airflow rate with almost linear proportionality. This is consistent with experimental observation in some other types of ventilated structures.[10,26] Figure 4(e) shows the contour plot of the absolute flow velocity at the horizontal mid-plane of the model for various inlet flow velocities. The air flowing across the ventilated channel can be clearly observed, demonstrating the air ventilation performance of the structure. Notice that the outlet flow is bent towards the boundary wall due to the asymmetric geometry of the structure, but without influencing the ventilation behavior. The ventilated channel has the percentage of opening 18%. It yields a smaller outlet velocity than that of the fully opening case (i.e., without the

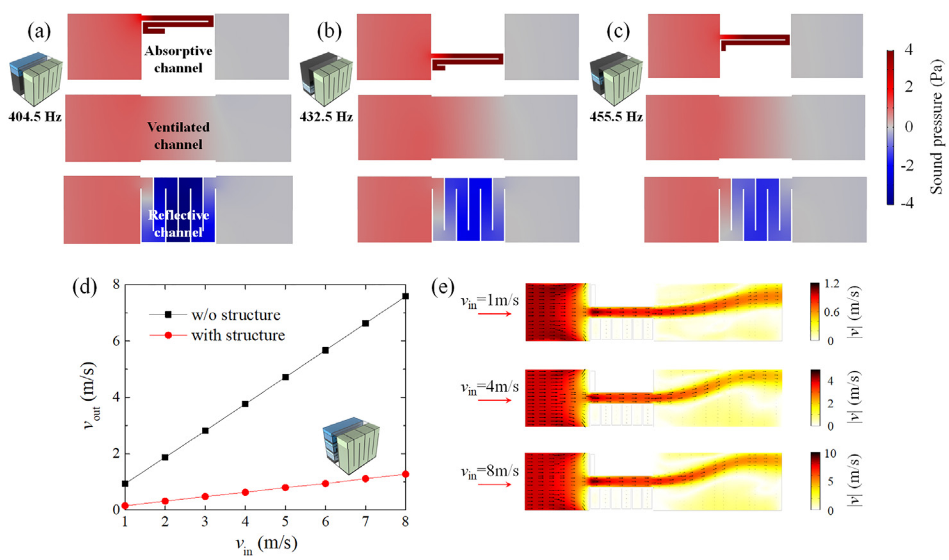

Fig. 4. (a)–(c) Acoustic pressure field distribution at the respective vertical mid-plane of absorptive, ventilated, and reflective channeling structures for three types of systems corresponding to Figs. 3(c)–3(e) with maximum absorption at frequencies of (a) 404.5 Hz, (b) 432.5 Hz, and (c) 455.5 Hz, respectively. Simulation results of the ventilation performance: (d) averaged outlet flow velocity against inlet velocities in cases with and without the sample structure, and (e) contour plots of the absolute flow velocity at the horizontal mid-plane of the model for various inlet flow velocities 1, 4, and 8 m/s.

structure), as shown by comparison results in Fig. 4(d). However, the proposed model holds the potential to further enlarge the ventilation opening through the design optimization.

4. Conclusions

In summary, we have proposed the channel-type structures capable of both high sound absorption and air ventilation. The model consists of two types of channeling structures, in which the reflective channel functions for the blockage of sound transmission, while the absorptive channel is used for absorbing sounds at low-transmission frequencies. The reflective and absorptive channels can be designed separately, allowing the decoupling-design strategy to be adopted for achieving the high sound absorption. Results have been demonstrated by theoretical, numerical, and experimental analyses. The model holds also the potential to expand the absorption bandwidth by combining different absorptive channels into the sample structure. The proposed method is potentially applicable to the engineering environment that demands noise absorption and air ventilation.

Acknowledgments

The authors acknowledge Professor Xiaoliang Wang for helpful discussions about CFD modeling. This work was supported by the National Natural Science Foundation of China (Grant Nos. 11632003, 11872111, 11991030, 11991033, 11622215) and 111 project (B16003).

References and Links

[1]M. Yang and P. Sheng, "Sound absorption structures: From porous media to acoustic metamaterials," Annu. Rev. Mater. Res. **47**(1), 83–114 (2017).

[2]H. Nguyen, Q. Wu, X. Xu, H. Chen, S. Tracy, and G. Huang, "Broadband acoustic silencer with ventilation based on slit-type Helmholtz resonators," Appl. Phys. Lett. **117**(13), 134103 (2020).

[3]R. Dong, M. Sun, F. Mo, D. Mao, X. Wang, and Y. Li, "Recent advances in acoustic ventilation barriers," J. Phys. D: Appl. Phys. **54**(40), 403002 (2021).

[4]Y. Li and B. M. Assouar, "Acoustic metasurface-based perfect absorber with deep subwavelength thickness," Appl. Phys. Lett. **108**(6), 063502 (2016).

[5]M. Yang, S. Chen, C. Fu, and P. Sheng, "Optimal sound-absorbing structures," Mater. Horiz. **4**(4), 673–680 (2017).

[6]X. Jiang, B. Liang, R-q. Li, X-y. Zou, L-l. Yin, and J-c. Cheng, "Ultra-broadband absorption by acoustic metamaterials," Appl. Phys. Lett. **105**(24), 243505 (2014).

[7]S. Huang, Z. Zhou, D. Li, T. Liu, X. Wang, J. Zhu, and Y. Li, "Compact broadband acoustic sink with coherently coupled weak resonances," Sci. Bull. **65**(5), 373–379 (2020).

[8]Y. Chen, G. Huang, X. Zhou, G. Hu, and C.-T. Sun, "Analytical coupled vibroacoustic modeling of membrane-type acoustic metamaterials: Plate model," J. Acoust. Soc. Am. **136**(6), 2926–2934 (2014).

[9]V. Romero-García, N. Jiménez, J.-P. Groby, A. Merkel, V. Tournat, G. Theocharis, O. Richoux, and V. Pagneux, "Perfect absorption in mirror-symmetric acoustic metascreens," Phys. Rev. Appl. **14**(5), 054055 (2020).

[10]X. Xiang, X. Wu, X. Li, P. Wu, H. He, Q. Mu, S. Wang, Y. Huang, and W. Wen, "Ultra-open ventilated metamaterial absorbers for sound-silencing applications in environment with free air flows," Extreme Mech. Lett. **39**, 100786 (2020).

[11]S. Kumar and H. P. Lee, "Labyrinthine acoustic metastructures enabling broadband sound absorption and ventilation," Appl. Phys. Lett. **116**(13), 134103 (2020).

[12]N. Jiménez, V. Romero-García, V. Pagneux, and J.-P. Groby, "Quasiperfect absorption by subwavelength acoustic panels in transmission using accumulation of resonances due to slow sound," Phys. Rev. B **95**(1), 014205 (2017).

[13]T. Lee, T. Nomura, E. M. Dede, and H. Iizuka, "Ultrasparse acoustic absorbers enabling fluid flow and visible-light controls," Phys. Rev. Appl. **11**(2), 024022 (2019).

[14]T. Lee, T. Nomura, and H. Iizuka, "Damped resonance for broadband acoustic absorption in one-port and two-port systems," Sci. Rep. **9**(1), 13077 (2019).

[15]T. Lee, T. Nomura, E. M. Dede, and H. Iizuka, "Asymmetric loss-induced perfect sound absorption in duct silencers," Appl. Phys. Lett. **116**(21), 214101 (2020).

[16]A. Merkel, G. Theocharis, O. Richoux, V. Romero-García, and V. Pagneux, "Control of acoustic absorption in one-dimensional scattering by resonant scatterers," Appl. Phys. Lett. **107**(24), 244102 (2015).

[17]H. Long, Y. Cheng, and X. Liu, "Asymmetric absorber with multiband and broadband for low-frequency sound," Appl. Phys. Lett. **111**(14), 143502 (2017).

[18]X. Wu, K. Y. Au-Yeung, X. Li, R. C. Roberts, J. Tian, C. Hu, Y. Huang, S. Wang, Z. Yang, and W. Wen, "High-efficiency ventilated metamaterial absorber at low frequency," Appl. Phys. Lett. **112**(10), 103505 (2018).

[19]L-j. Li, B. Zheng, L-m. Zhong, J. Yang, B. Liang, and J-c. Cheng, "Broadband compact acoustic absorber with high-efficiency ventilation performance," Appl. Phys. Lett. **113**(10), 103501 (2018).

[20]N. Jiménez, V. Romero-García, V. Pagneux, and J.-P. Groby, "Rainbow-trapping absorbers: Broadband, perfect and asymmetric sound absorption by subwavelength panels for transmission problems," Sci. Rep. **7**(1), 13595 (2017).

[21]C. Fu, X. Zhang, M. Yang, S. Xiao, and Z. Yang, "Hybrid membrane resonators for multiple frequency asymmetric absorption and reflection in large waveguide," Appl. Phys. Lett. **110**(2), 021901 (2017).

[22]M. Yang, C. Meng, C. Fu, Y. Li, Z. Yang, and P. Sheng, "Subwavelength total acoustic absorption with degenerate resonators," Appl. Phys. Lett. **107**(10), 104104 (2015).

[23]See supplementary material at https://www.scitation.org/doi/suppl/10.1121/10.0009919 for the analytic expression of effective impedance and sound speed of narrow channels, the theoretical derivation of acoustic scattering coefficients, geometric parameters and acoustic testing method of samples, as well as the CFD modeling details.
[24]C. Chen, Z. Du, G. Hu, and J. Yang, "A low-frequency sound absorbing material with subwavelength thickness," Appl. Phys. Lett. **110**(22), 221903 (2017).
[25]M. Sun, X. Fang, D. Mao, X. Wang, and Y. Li, "Broadband acoustic ventilation barriers," Phys. Rev. Appl. **13**(4), 044028 (2020).
[26]X. Xiang, H. Tian, Y. Huang, X. Wu, and W. Wen, "Manually tunable ventilated metamaterial absorbers," Appl. Phys. Lett. **118**(5), 053504 (2021).